IEEE Access
Multidisciplinary | Rapid Review | Open Access Journal

Received May 29, 2019, accepted June 13, 2019, date of publication July 1, 2019, date of current version September 16, 2019.

Digital Object Identifier 10.1109/ACCESS.2019.2925900

A Dehazing Algorithm Based on Local Adaptive Template for Transmission Estimation and Refinement

LU XU[1], YING WEI[1,2], BIN HONG[1], AND WEI YIN[1]
[1]School of Information Science and Engineering, Northeastern University, Shenyang 110819, China
[2]Key Laboratory of Medical Imaging Calculation of the Ministry of Education, Northeastern University, Shenyang 110179, China

Corresponding author: Ying Wei (weiying@ise.neu.edu.cn)

This work was supported by the National Natural Science Foundation of China under Grant 61871106.

ABSTRACT Outdoor images are vulnerable to environment and may suffer various distortions. Therefore, preprocessing for images captured in bad weather is particularly important for computer vision system. One of the most common conditions is haze. Image dehazing, especially single image dehazing is a challenging topic since it's an ill-posed problem and needs to rely on extra information or prior. In this paper, we discussed the shortcomings of existing algorithms and proposed a novel step called Local Adaptive Template. The template is used in transmission estimation and transmission refinement. Starting from the target pixel, the template is extracted under the guidance of the similarity function and only contains pixels related to the center point, thus avoids the influence of adjacent objects, even those with blur edges. We then used the template to improve the Dark Channel Prior(DCP) and the Guided Filter(GF) respectively, and effectively avoided the block effect in DCP and the blur in GF. The obtained transmission map is much more accurate, and free from the halo effect. The dehazing result is much clearer and still looks natural without haze residual. Experiments on natural images and synthetic images show that our method achieves better dehazing results than several state-of-art algorithms and can adapt to different situations.

INDEX TERMS Local adaptive template, halo effect, haze residual, dark channel prior, guided filter.

I. INTRODUCTION

Under bad weather conditions, light will be scattered by suspended particles such as fog or haze. Light reflected by the target objects will decay, meanwhile the atmospheric light will get mixed with light captured by the optical sensor [1]–[3]. Both of them will eventually result in degradation of digital image. The degradation mainly reflects in local contrast decreased and scene detail illegible etc. Therefore, with the development and maturity of computer vision, image dehazing technology is receiving more and more attention.

Currently, image processing methods for haze weather can be roughly divided into two categories [4], [5]. One is based on image enhancement, the other is based on physical models. Image enhancement methods aim at the faults of haze images, and apply existing enhancement algorithms to dehazing [6]–[10]. These algorithms can enhance image contrast, highlight scene features and emphasize valuable information. However, they can not adapt to the changes in scene depth, and may cause distortion and lose information. Other algorithms make use of physical models [11], [12], such as the atmospheric scattering model to recover the images. Some of them depend on special equipment to obtain scene depth information. In recent years, a number of algorithms based on prior knowledge have emerged. Images reconstructed by physical model are closer to the original scenes. Also, they can adapt to the depth change of complex scenes, and obtain more structure information.

The algorithm we discussed in this paper is one of the physical model based methods. It's based on the algorithm proposed by He who goes through lots of outdoor clear images, and finds out that in most of the natural images, most pixels other than the sky area have at least one color channel with very low intensity value [13]. Such characteristic can be used to estimate the transmission map, and with the help of soft mapping algorithm, the haze free image can be easily achieved. However, the complexity of the algorithm and the

The associate editor coordinating the review of this article and approving it for publication was Yongqiang Zhao.

deficiencies of the result all limit its application. Recently, there have been lots of improvements in time complexity caused by soft mapping. Bilateral filtering and median filtering are used to improve the efficiency of the algorithm. The Guided Filter proposed by He himself can efficiently solve the problem [14], but it may also cause blur around the edge region.

To obtain better dehazing results, some improvements on the template of Guided Filter and Dark Channel Prior have been proposed. They aim to solve the block effect in DCP and the blur in GF. Reference [15] takes the minimum value among RGB channels as the transmission value of the point. It can completely avoid the block effect, but the resulting transmission is too small and may cause serious distortion. Among all the templates that cover the target pixel, [16] finds the window with the smallest variance value in order to avoid the blur in GF. However, in some complex areas, fixed window size may not be able to avoid interference from adjacent objects. Reference [17] extracts the template from four directions, up, down, right and left. Length in each direction is counted respectively, but information on other locations is ignored. Reference [18] proposes a ''two-level local adaption'' to guide the filtering approach.

In this paper we focused on the halo effect, and proposed a Local Adaptive Template to improve both the transmission estimation and transmission refinement. The rest of the paper is: In Sec.2, the atmospheric scattering model, Dark Channel Prior and Guided Filter are briefly introduced. In Sec.3, the causes of the halo effect are discussed. Sec.4 proposes the Local Adaptive Template and introduces RTV(Relative Total Variation) to image dehazing, besides our final dehazing method is proposed. Experiments are shown in Sec.5. Sec.6 gives the conclusion.

Main contributions: Instead of estimating and refining the transmission map in a square region, we proposed a novel template extraction approach called ''Local Adaptive Template'':

- The template only extracts pixels closely related to the target point and can adapt to different kinds of situations.
- RTV is introduced to image dahazing for the first time to minimize the effect of texture.
- The proposed method can still work under noise conditions.
- We use the template in DCP and GF, and manage to obtain clear images free from the halo effect.

II. RELATED WORKS

In this section, we introduced the underlying model of image dehazing and paid attention to some of the existing algorithms we used in this paper.

A. HAZE MODELING

Under haze condition, the atmospheric scattering model can be described as [19]:

$$I(x) = J(x)t(x) + A(1 - t(x)) \tag{1}$$

$t(x) = e^{-\beta d(x)}$ is the transmission, x is the location of the current pixel, β is the atmospheric scattering coefficient, $d(x)$ is the depth of the scene. $I(x)$ represents the input image, while $J(x)$ represents the haze free image, and A is the global atmospheric light. The atmospheric scattering model consists of two components. The first one $J(x)t(x)$ is the direct attenuation. It represents the un-refracted part of the light from the scene, and it exponentially decays as the scene depth increases. The second part $A(1 - t(x))$ is the airlight item, which represents the part of atmospheric light involved in image.

Algorithms based on atmospheric scattering model aim to recover clear image $J(x)$ from haze image $I(x)$. Since the mathematical expression of the atmospheric scattering model is an underdetermined equation, only the haze image $I(x)$ is known. In order to recover haze-free image $J(x)$, we first need to estimate global atmospheric light A and transmission $t(x)$.

B. DARK CHANNEL PRIOR

The Dark Channel Prior is based on the following observation on outdoor haze-free images: In most of the non-sky patches, at least one color channel has some pixels whose intensities are very low and close to zero. Equivalently, the minimum intensity in such a patch is close to zero. As shown in Eq.(2):

$$J^{dark}(x, y) = \min_{y \in \Omega(x)} \left(\min_{c \in \{r,g,b\}} \left(J^c(y) \right) \right) \to 0 \tag{2}$$

where J^c is a color channel of J and $\Omega(x)$ is a local patch centered at x (usually 7×7 or 15×15).

C. GUIDED FILTER

Guided Filter is an effective method to refine the transmission map.

Supposing the guidance image is I, the image to be filtered is p and the resulting image is q. The local linear model of the Guided Filter is as follows:

$$q_i = a_k I_i + b_k, i \in \omega_k \tag{3}$$

where ω_k is a neighborhood centered at pixel i with radius k, and a_k,b_k are fixed values within the neighborhood, which is the basic condition for the formula to be established in a local window.

The weighted-average filters solve a linear system in this form:

$$\nabla q = a \nabla I \tag{4}$$

The process of solving the filtering result is equivalent to minimizing the Eq.(5):

$$E(a_k, b_k) = \sum_{i \in \omega_k} \left((a_k I_i + b_k - pi)^2 + \varepsilon a_k^2 \right) \tag{5}$$

The first term is the second-order fidelity which guarantees the establishment of the local linear model with the minimum difference between q and p. The second term is the regular term, which is used for rounding off the large a_k, so ε must be bigger than 0.

When calculating linear coefficients in a window, one pixel may be found in multiple windows at the same time, that is, each pixel can be described by multiple linear functions. So, when calculating the output value at a certain point, the original Guided Filter averages all the linear function values that contain that point, as shown in Eq.(6):

$$q_i = \frac{1}{|\omega|} \sum_{k:i\in\omega_k} (a_k I_i + b_k) = \bar{a}_i I_i + \bar{b}_i \tag{6}$$

III. HALO EFFECT ANALYSIS

In this section, we analyzed the possible causes of halo effect, to be more specific, the block effect in DCP and the blur in GF.

A. HALO EFFECT IN DCP

Dark Channel Prior algorithm has its own limitation. The algorithm suffers serious block effect. Some post-processing can help with the problem, but the block effect still affects the final result.

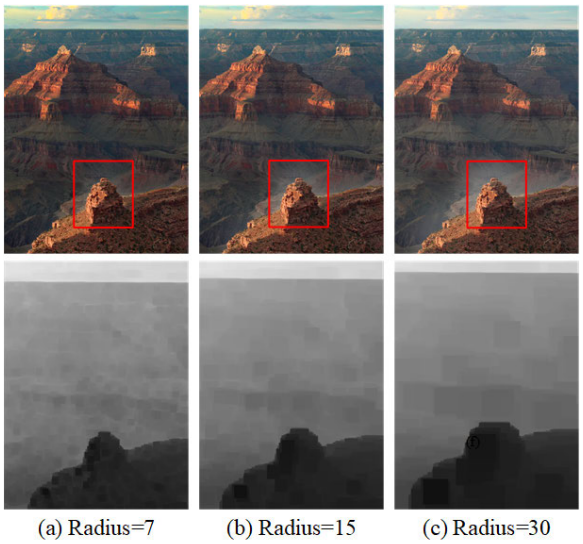

FIGURE 1. Block effect analysis: Dehazing results and transmission maps under different window sizes.

Fig.1 shows the dehazing results and transmission maps with different window sizes. As the window grows, more pixels are given the wrong transmission values, and the process results suffer more halo effect. WeÂ use it as a proof to show that the block effect is one of the major causes of halo effect. As the window grows, the block effect gets worse, so is the halo effect, as can be seen from Fig.1. It's quite obvious in the region we marked.

B. HALO EFFECT IN GF

Another possible reason that may cause halo effect is the Guided Filter. The center window scheme in Guided Filter can cause blur at the edges, as shown in Fig.2. Fig.2(b) gives the result of the Guided Filter using input image itself as the guidance image. Fig.2(c)(d) shows the change of the image.

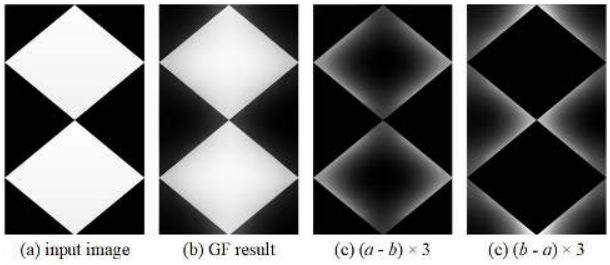

FIGURE 2. Guided filter smoothing.

The smoothing operation allows the white and black parts to penetrate each other. In transmission refinement this eventually leads to the halo effect in the dehazing result. Such characteristic once again proves the importance of the initial estimation accuracy: when the Guided Filter corrects the error, it's more likely to disperse the error to the surroundings, resulting in halo effect.

The halo effect is actually a kind of haze residual. As can be seen from the above analysis, the halo effect is caused by both the DCP and the GF. And in both algorithms, the estimation errors are caused by the partial window covering the pixels of adjacent objects. Therefore, if a more accurate window selection method can be proposed, the errors and the halo effect can be effectively avoided, and we may achieve better dehazing results with much less haze residual.

IV. PROPOSED METHOD

In this section, our algorithm was introduced. Firstly, we introduced the two key steps of the algorithm, and then the full algorithm.

A. LOCAL ADAPTIVE TEMPLATE

To avoid the halo effect, we proposed the Local Adaptive Template to extract a more accurate neighborhood for each pixel.

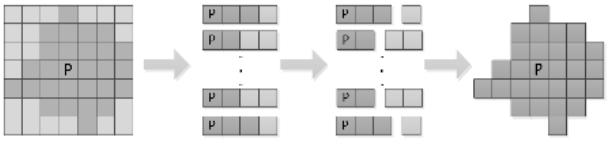

FIGURE 3. Illustration of the local adaptive template.

Fig.3 is the flowchart of the proposed Local Adaptive Template. As shown in Fig.3, for the target pixel p we first took p and each pixel on the square boundary as the endpoints, and extracted the pixels in each direction. In order to make sure the template only contains pixels that are related to p, we then determined the length in each direction adaptively. The final template can be obtained by jointing all the selected pixels together. As can be seen in Fig.3, the output of the Local Adaptive Template only contains gray pixels, which are clearly related to p.

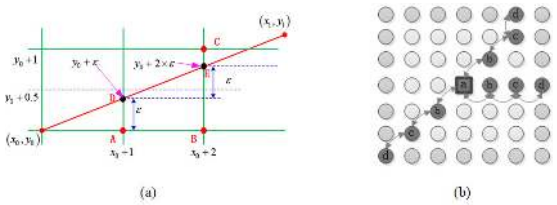

FIGURE 4. Extracted pixels in each direction.

The detail of pixel extraction is shown in Fig.4. Fig.4(a) shows the workflow of Bresenham algorithm [20]. Fig.4(b) shows how the algorithm works in template extraction. Brensenham algorithm extracts the most appropriate path between the initial and final pixels. Therefore, we took the target pixel as the initial pixel and the point on the square boundary as the end pixel to extract the path in turn. Through analysis, it is easy to know that the method can ensure the extraction result covers all the pixels.

After extracting the pixels, the similarity between the pixels in the template and the central pixel needs to be determined adaptively so as to determine the scope of the template in each direction, that is, the length. As for region with high similarity, it's more likely to be texture, and the length is expected to be large. Otherwise, for the region with small similarity, it's more likely to be boundary, and the length is expected to be small. Finally, the results in all directions are integrated to obtain a similar neighborhood region adaptively changing with the gradient information.

For a random pixel $p(p \in I)$, the pixel in each direction needs to be extracted and the similarity in each line is supposed to be calculated, so as to improve the transmission estimation result. Let the position of pixel p be (x, y), and the pixel value be $I(x, y)$. Taking the positive direction of x as an example, the similarity function is [21]:

$$\overset{m}{I}_p = (1-\alpha)\overset{(m-1)}{I}_p + \alpha I(x+m, y) \tag{7}$$

Here, $\overset{m}{I}_p$ represents the similarity of the mth point in the x^+ direction of point p, and we define $\overset{m}{I}_p = I(x, y)$. α is the adjustment parameter, which is used to adjust the calculated similarity degree. Since the length of the line segment in each direction in the area is fixed at k, the range of m is $[0, \frac{k-1}{2}]$, and $I(x+m, y)$ is the pixel value of point $(x+m, y)$. When the difference between the values of a pixel and its previous pixel is less than the threshold τ, we consider that all the pixels between the pixel and the center point p are similar. The expression is as follows:

$$\begin{cases} \delta\left(I(x+m, y), \overset{(m-1)}{I}_p, \tau\right) = 1, & |I(x+m, y) - \overset{(m-1)}{I}_p| \le \tau \\ \delta\left(I(x+m, y), \overset{(m-1)}{I}_p, \tau\right) = 0, & else \end{cases} \tag{8}$$

$\delta\left(I(x+m, y), \overset{(m-1)}{I}_p, \tau\right)$ is a marker bit, and τ is the similarity threshold. With the increase of m, the similarity of pixels in the region decreases. Until the case of $\delta\left(I(x+m, y), \overset{(m-1)}{I}_p, \tau\right) = 0$, the farthest similar pixel is found. Thus, the length h can be calculated as shown in Eq.(9):

$$h = \max\left(m | \delta\left(I(x+m, y), \overset{(m-1)}{I}_p, \tau\right) = 1\right) \tag{9}$$

The final template is shown in Fig.5, compared to the traditional square region, it avoids being disturbed by the boundary and the neighboring objects. The gray part and the white part in the picture belong to two objects which are adjacent to each other. The square template in Fig.5(a) covers a large number of pixels on the gray object, while the Local Adaptive Template in Fig.5(b) only contains the pixels on the white object.

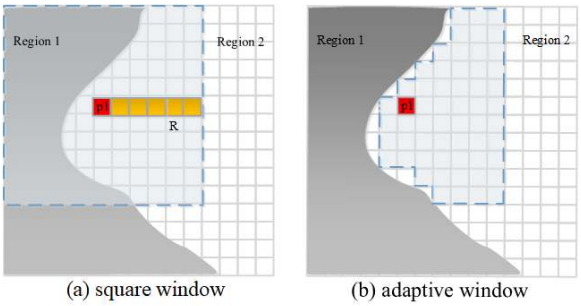

(a) square window (b) adaptive window

FIGURE 5. The extracted templates.

B. PARAMETER DETERMINATION

Natural images have a lot of textures. These textures may affect the results of template extraction. Therefore, whether the parameters of similarity function can be reasonably set has a great influence on the results. If the template gets too large, the result of the algorithm will be similar to that of the square neighborhood. On the contrary, the estimated transmission value may be too small, which will distort the final dehazing image. Therefore, fixed parameters do not fit the whole image.

In this section, we introduced the Structure Extraction from Texture via Relative Total Variation and used it to determine the parameters in the similarity function [22]. The algorithm can remove the texture information of the image and preserve the complete structure. Applying the algorithm extraction results to the template determination can avoid the influence of image texture while accurately estimating the transmission values.

The structure extraction from texture via Relative Total Variation believes that an image is a linear combination of structure information and texture information, as shown in Eq.(10):

$$I = S + T \tag{10}$$

I represents the input image. S represents its structure part, that is, the large-scale part, and it has the characteristic of piecewise smooth. T represents the texture part of the image, mainly the small-scale details of the image and the noise.

The structure extraction of the image is to extract the structure part S from the original image I. Based on this idea, we can get the basic model of image structure extraction:

$$\min \frac{1}{2}||S - I||^2 + \lambda prior \tag{11}$$

The first part is the data fidelity item, keeping S as close to I as possible to preserve the structure information of the image. The second part is the prior item, where λ is the parameter to balance the first and second item. Xu's method extracts the structure based on RTV which is the ratio of the Windowed Total Variation and Windowed Inherent Variation. For a pixel p, RTV can be defined as:

$$RTV(p) = \Big(D_x(p)/\big(L_x(p) + \varepsilon\big) + D_y(p)/\big(L_y(p) + \varepsilon\big)\Big) \tag{12}$$

ε is a constant bigger than 0, used to ensure that the denominator is not zero. D is the Windowed Total Variation and L is the Windowed Inherent Variation. D and L are defined as follows:

$$\begin{cases} D_x(p) = \sum\limits_{q \in R(q)} g_{p,q} \big|\big(\partial_x S\big)\big| \\ D_y(p) = \sum\limits_{q \in R(q)} g_{p,q} \big|\big(\partial_y S\big)\big| \\ L_x(p) = \big|\sum\limits_{q \in R(q)} g_{p,q} \big(\partial_x S\big)\big| \\ L_y(p) = \big|\sum\limits_{q \in R(q)} g_{p,q} \big(\partial_y S\big)\big| \end{cases} \tag{13}$$

q represents all the pixels in the window, $g_{p,q}$ represents the weight function formed as:

$$g_{p,q} \propto \exp\left(-\frac{(x_p - x_q)^2 + (y_p - y_q)^2}{2\sigma^2}\right) \tag{14}$$

σ is the Gaussian standard deviation.

As can be seen from Eq.(13), for a target pixel, Windowed Total Variation is the weighted sum of the absolute value of the gradient in the neighborhood, and Windowed Inherent Variation is the absolute value of sum of the gradient in the neighborhood.

Therefore, the value of Windowed Total Variation depends on the gradient value of the neighborhood pixels, while the value of Windowed Inherent Variation depends on both the gradient value and the gradient direction of the neighborhood pixels. Intuitively, the structure of the image has a similar gradient direction in a local area. On the contrary, the texture details are more complex and the gradient directions are different. RTV combining Windowed Total Variation and Windowed Inherent Variation together can achieve the best separation results.

As can been seen from $t(x) = e^{-\beta d(x)}$, transmission is only related to the depth and the extinction coefficient, so it shouldn't be influenced by the texture. Hopefully by introducing RTV, α in Eq.(7) can be kept small near the main structure to maintain the edge, and accordingly a larger α can be obtained in the texture area to avoid the influence of the texture. In order to achieve this, a threshold is set for RTV. When the RTV of the target pixel is larger than the threshold, it is regarded as a texture area, and α of the position is set to a large value. On the contrary, the area is regarded as the main structure area, and α of the position is set to a small value.

C. DEHAZING METHOD

Until now, we can propose the algorithm in this paper. Our algorithm is based on Dark Channel Prior and Guided Filter, and is designed to avoid the halo effect.

According to the analysis in Sec.3, the halo effect in dehazing results mainly has two main causes. One is due to the block effect caused by the square neighborhood in DCP, and the other is due to the blur at the boundary in GF. Thus, we used the proposed Local Adaptive Template to improve the two algorithms to make them more suitable for image dehazing tasks. First, the Local Adaptive Template is used to replace the square neighborhood in DCP. When calculating the dark channel value, the pixels are selected from the template. So, with Ω_t representing the extracted template, the algorithm becomes:

$$J^{dark}(x, y) = \min_{y \in \Omega_t(x)} \left(\min_{c \in \{r,g,b\}} \big(J^c(y)\big)\right) \to 0 \tag{15}$$

Ω_t represents the extracted template.

In Guided Filter, all the results in the window covering the target pixel need to be averaged to get the output, this is what we call the central window scheme. However, it may leads to the blur at the boundary. Therefore, we adopted the Local Adaptive Template instead of the existing central window scheme. With Ω_t representing the extracted template, the average in GF becomes:

$$q_i = \frac{1}{|\Omega_t|} \sum_{k: i \in \Omega_{tk}} (a_k I_i + b_k) = \bar{a_i} I_i + \bar{b_i} \tag{16}$$

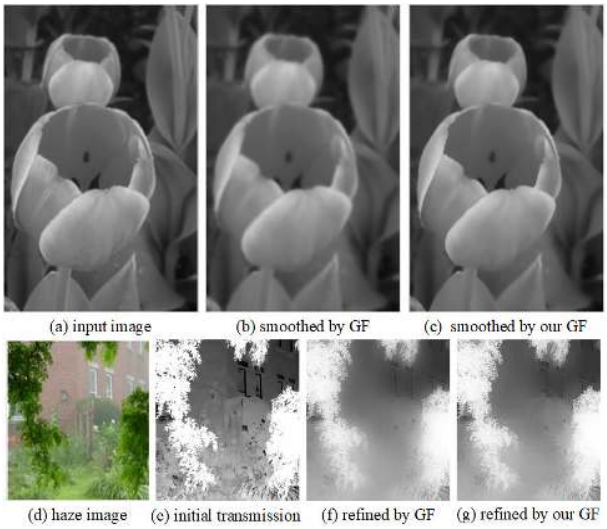

FIGURE 6. Smoothing and refining results.

Fig.6 shows the process results of our Guided Filter in image smoothing and transmission refinement. Compared to

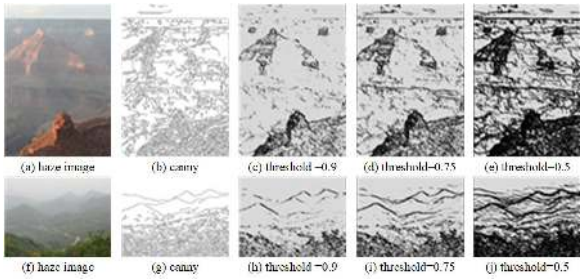

FIGURE 7. α **distribution with different RTV parameters.**

the original Guided Filter, the one improved by Local Adaptive Template can obtain more structure information.

After obtaining the transmission, we still need to calculate the atmospheric light value. Atmospheric light estimation is an important part in image dehazing. The estimation result directly affects the final output. In haze images, the existence of haze always causes the brightness to increase. Therefore, it is considered that the area with higher brightness is more likely to be a haze area. Based on this idea, He *et al.* [13] first selects the brightest 0.1% points in the dark channel map, then selects the brightest point from these pixels as the atmospheric light value. However, this method is vulnerable to bright subjects in some conditions.

In this paper, we used a hierarchical searching method based on the quad-tree subdivision which is proposed by Kim *et al.* [16]. The method first divides the image into four candidate regions, computes the difference between the mean value and the standard deviation in each region, selects the best from the four regions according to the result and repeats the above operation until the size of the obtained region is smaller than the preset threshold.

Then the resulting area is used as a candidate area. We selected the brightest pixel, that is, the point at which $||\big(I_r(p), I_g(p), I_b(p)\big) - (255, 255, 255)||$ takes the minimum value as the atmospheric light. Through the region selection operation, the algorithm narrows the search area to a more bright and smoother area, effectively avoiding the influence of other objects and making the final atmospheric light value more accurate.

The method consists of 8 steps totally and it can be summarized as follows:

1) Extract pixels in each direction using Bresenham algorithm.
2) Apply RTV to adjust the similarity degree α.
3) Apply the similarity function in Eq.(3)-(5) to determine the length h for each direction.
4) Form the Local Adaptive Template Ω_t.
5) Estimate the transmission map with Eq.(15).
6) Refine the transmission map with Eq.(16).
7) Estimate the atmospheric light.
8) Obtain clear images according to the atmospheric scattering model.

V. EXPERIMENTAL RESULT

In this section, we showed the effectiveness of the proposed method. First, we analyzed the dehazing performance under noise condition, and compared our dehazing results with Dark Channel Prior.

Then, we compared our dehazing results with several state-of-art algorithms, using real-world images with dense and light haze and synthetic images. The subjective and objective analysis is given.

A. ALGORITHM ANTI-NOISE ABILITY ANALYSIS

It's worth noticing that the original Dark Channel Prior based dehazing algorithm may be easily affected by noise especially by dark noise points, because any region including the noise point may choose it to be the dark channel value. In practice, noise is inevitable. This shortcoming greatly limits the application of the algorithm.

To give the anti-noise ability of the proposed algorithm, we first analyzed the distribution of the most related parameter α. Fig.7 shows the distribution of α calculated by RTV. The results clearly show the differences between RTV and edge detection. We want α in the main structure to be relatively small, and α in the texture area to be relatively large.

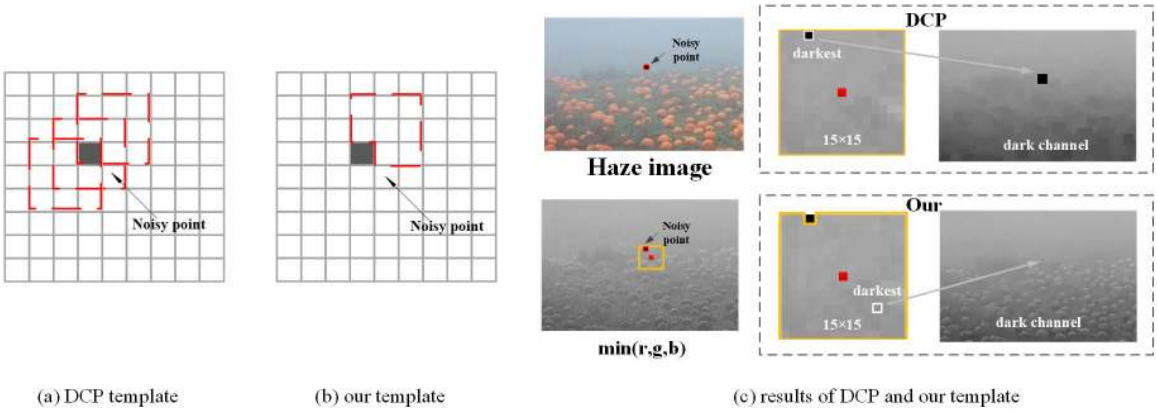

FIGURE 8. **Anti-noise ability analysis in local area.**

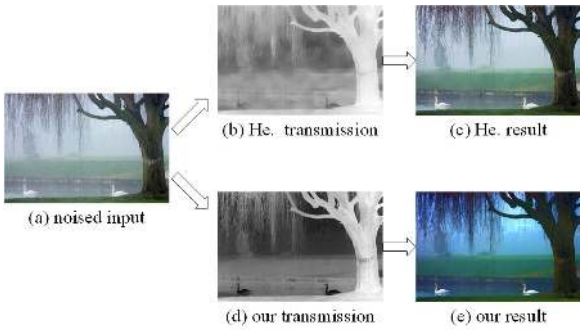

FIGURE 9. Contrast of dehazing results affected by noise.

This ensures that the similarity function effectively distinguishes the structure and texture, further, avoids DCP to cover the adjoining items. As can be seen from Fig.7, the threshold effectively distinguishes the texture and the main structure edges. And as the threshold increases, more edges are considered as the main structure. By adjusting α, the algorithm can adapt to different dehazing requirements.

Then we analyzed the algorithm anti-noise ability. Fig.8 (b) gives an example of how our method obtains correct transmission values around a noise point, and Fig.8(a) shows how DCP fails on these pixels. We used a 3×3 region as an example. As can be seen from Fig.8(a), once a noise point occurs, all windows around it will take the value of the noise point as the dark channel value, which means it will form a 3×3 black square on the DCP map. In Fig.8(b), the extracted template does not contain the noise point, so pixels around the noise point will still get the correct DCP values.

In Fig.8(c), the above problems are analyzed from the perspective of the whole picture. A black pixel is added to an image. The transmission estimation results show the difference. The original Dark Channel Prior produces a large black block around the noise point, while the improved algorithm is not influenced, and estimates the transmission accurately.

Dehazing experiments on the haze image are shown in Fig.9. We added salt and pepper noise into a common used haze image, and used DCP and our method to enhance the image. As can be seen, since the noise adds a lot of dark points into the haze image, DCP tends to take them as the dark channel values, and the obtained transmission map has many bright blocks. After refined by GF, the error spreads into the whole image and leads to serious haze residual. In contrast, our method manages to obtain accurate dark channel values by eliminating the noise points in template extraction phase, and provides a clear dehazing result.

B. COMPARISON OF DIFFERENT ALGORITHMS

Fig.10(a) shows the results of some classical algorithms. The results of [6] greatly improve the visual quality of the images, but there are haze residuals throughout the images with noticeably distorted colors. The algorithm based on Retinex deals with the haze images from the perspective of enhancement [23]. However, it suffers serious over-enhancement especially in the nearby view, which affects the results of

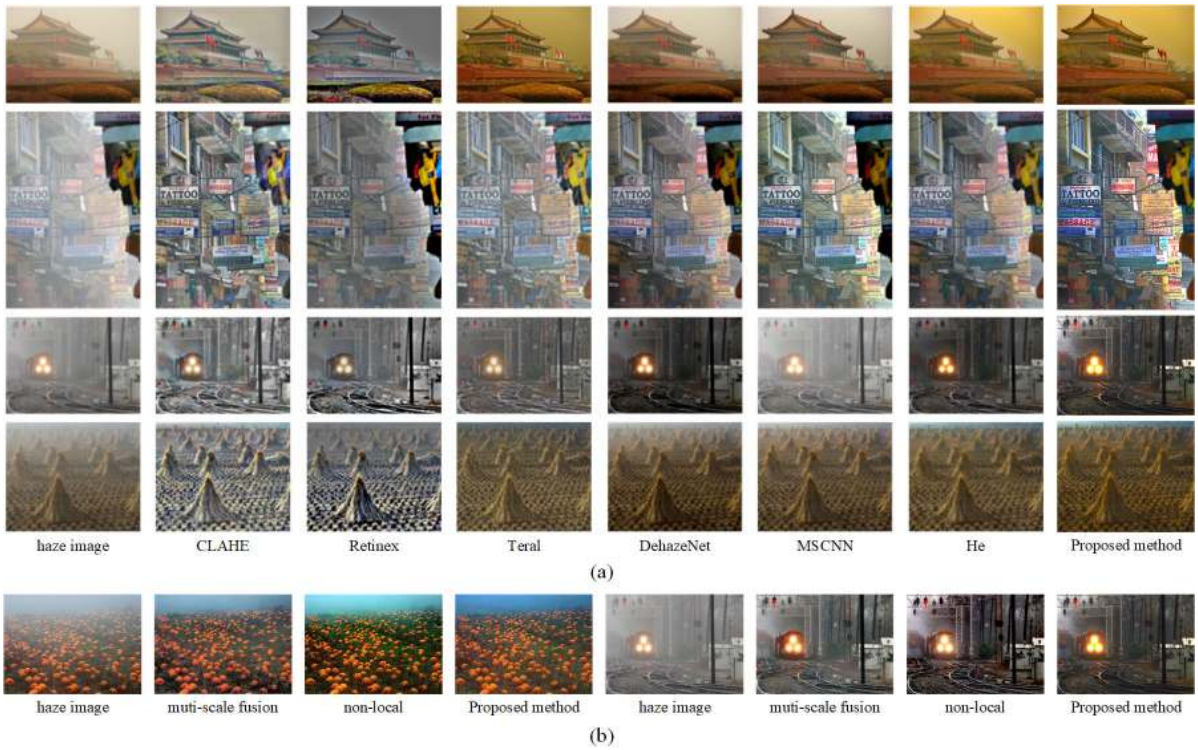

FIGURE 10. Dehazing results of different algorithms.

the algorithm. Teral and Hautiere [24] algorithm can significantly improve the image quality, but the visual effect is poor and noise is introduced. The results of He *et al.* [13], [14] algorithm are more natural, but they are affected by the halo effect. Deep learning based algorithms, DehazeNet [25] and MSCNN [26], achieve great visual effect, but still suffer serious haze residual. The proposed algorithm in this article performs better at the details, which is evident from the third and fourth image perspectives. At the same time, in the first image, the proposed algorithm effectively avoids the halo effect that He algorithm produces around the building.

In Fig.10(b), we compared our algorithm with other two state-of-art methods. Dehazing based on multi-scale fusion [27] proposes a novel strategy to fuse the results of two image enhancement methods. Reference [28] proposes a novel haze-line theory for image dehazing. As can be seen from the results, our method obtains clear images with higher saturation compared to [27]. The dehazing results of [28] have vivid color and rich details, but the results suffer color shift, while our results still have the similar color with the input images.

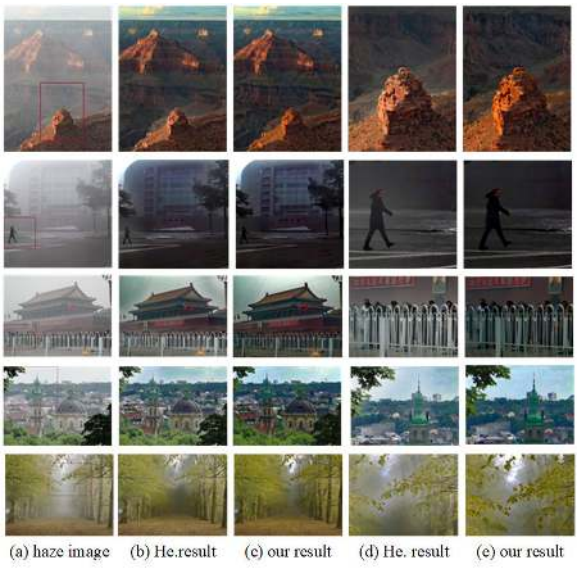

FIGURE 11. Halo effect analysis.

In Fig.11, our algorithm is further compared with DCP, especially areas with rapidly changing depth in the image. He *et al.* [13], [14] algorithm estimates the transmission inaccurately at the boundary since the dark channel results are affected by block effect, and the centered window scheme in the Guided Filter also results in blurred boundary. Finally, there is a large error in the estimated transmission at the position where the depth changes rapidly, resulting in halo effect. The improved algorithm in this paper starts from two aspects, which make the calculated transmission more accurate at the boundary, so as to effectively improve the halo effect. At the same time, more edge information is reserved during the computation of the dark channel, which further

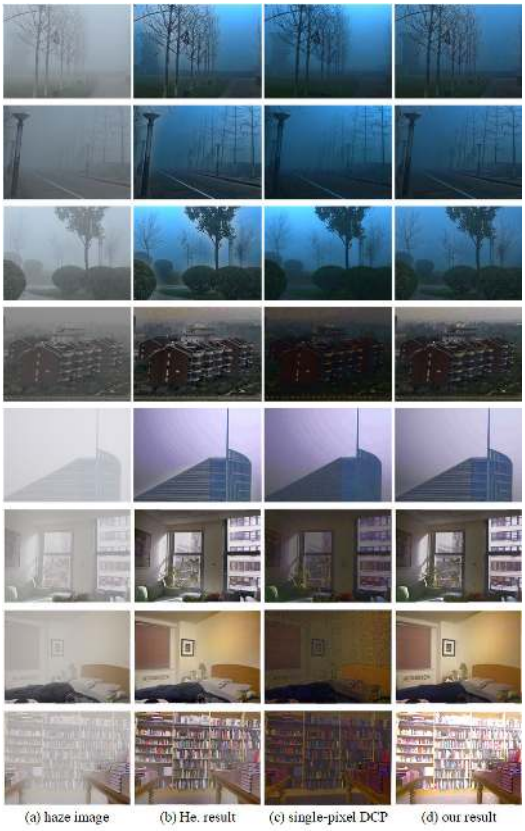

FIGURE 12. Result comparison of DCP, SDCP and our algorithm.

enriches the details of the final processing result. As shown in Fig.11, DCP results obviously have haze residual at the close-range locations and at the boundary with the distant mountains, while the proposed method doesn't.

In Fig.12 the proposed method is compared with the Single-pixel DCP [15]. Natural images and synthetic images are both used. The natural images are from the dataset of [29]. These images have close objects with large depth differences, so they can be easily affected by halo effect. The synthetic images are based on the NYU depth dataset [30]. We randomly selected 30 images and generated synthetic images of heavy haze. Both of the Single-pixel DCP and the proposed algorithm can achieve haze free images without halo effect. However, the single-pixel DCP suffers significantly over-enhanced, and the results are dark, resulting in the loss of a lot of information. The algorithm of this paper is able to achieve clear images by combining the advantages of both the single-pixel DCP and He algorithm. The processing results completely remove the influence of haze, and the scenes are much brighter and retain more information.

We also calculated the index of the synthetic images in Fig.12. The results are showed in Fig.13 and they once again prove that our results contain more information. The SSIM index also shows that the structures of our results are closer to those of the input images. Although SDCP also achieves better results than DCP, it lags behind this paper in spatial frequency and suffers serious over-enhancement.

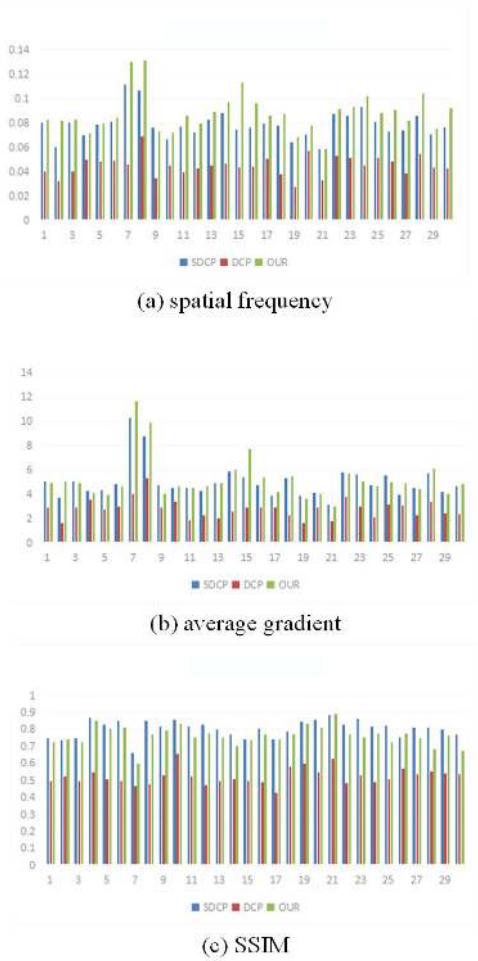

FIGURE 13. Synthetic image results analysis.

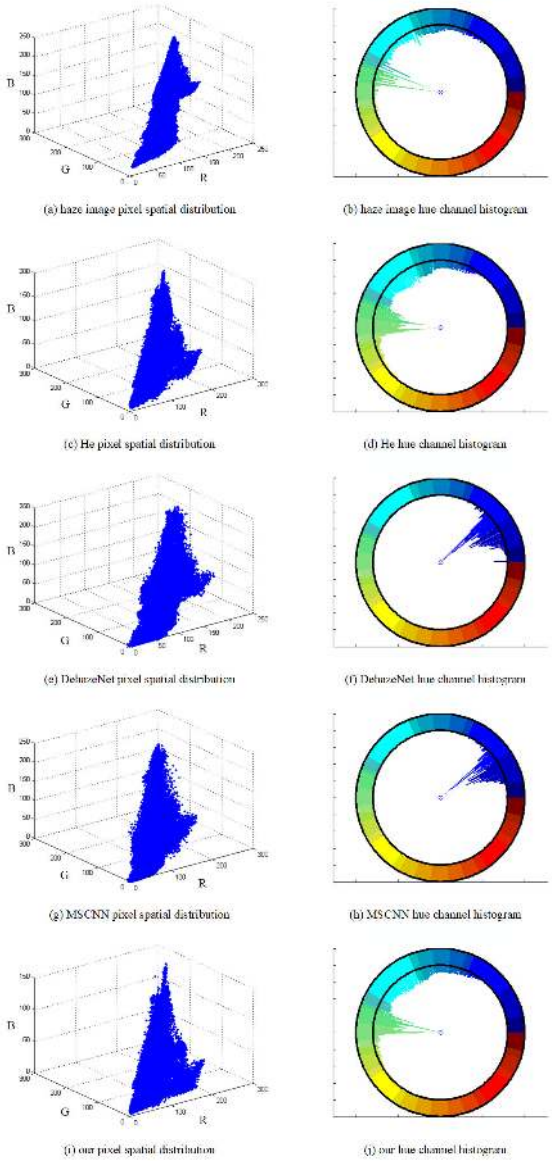

FIGURE 14. Image intrinsic property analysis.

Besides, we analyzed the intrinsic features of haze images. Take the image of Tiananmen Square in Fig.10 as an example. 3D scatter of RGB channel and hue mapping are shown in Fig.14. 3D scatter of RGB channel reveals the spatial distribution of the colors. The more haze the image has, the lower dynamic range the 3D scatter of the color channel is. It can be easily told that our results have the largest dynamic range. Hue shift is one of the most obvious features in haze images. Color histogram of a haze image is more centralized. Compared to other algorithms, our results and He results have broader distributions, and the color histograms are closer to that of the input haze image.

Then average gradient and spatial frequency of the images in Fig.10 are evaluated. The average gradient indicates the degree of clarity of the image, reflecting the ability to express the contrast of the image details. The larger the value is, the better the effect of the image dehazing is and the clearer the texture is. The spatial frequency indicates the change of the pixel value of the image in space, it is large in the region where the gray value is abrupt such as the edge and the noise, and it is small in the region where the gray value changes gently. It can reflect the complexity of the details to a certain extent. The higher the spatial frequency is, the more obvious the image details are. As can be seen from Table 1 and Table 2, the proposed method achieves higher average gradient than other algorithms. DehazeNet gets a better spatial frequency in the second test image. However, the result is significantly over-enhanced at the close scene. Another thing worth noticing is that the deep learning based algorithms achieve better results in sky region. This is due to the limitation that the DCP algorithm does not hold in the sky region.

DCP claims that low-intensity pixels in at least one color channel often exist in most of the local regions. To further evaluate the results of our dehazing method, we took 17 images that are common used in image dehazing task. We calculated the number of pixels with low dark channel

TABLE 1. Average gradient of Fig.10.

	He	DN	MSCNN	Ours
1	7.5981	7.1638	7.2378	**8.8977**
2	3.6407	3.5615	3.3965	**3.9691**
3	10.381	10.483	12.9250	**13.0122**
4	4.8006	4.9845	3.8490	**5.6339**

TABLE 2. Spatial frequency of Fig.10.

	He	DN	MSCNN	Ours
1	0.0781	0.0788	0.0757	**0.0891**
2	0.0456	**0.0555**	0.0469	0.0520
3	0.1326	0.1337	0.1693	**0.1806**
4	0.0499	0.0600	0.0417	**0.0647**

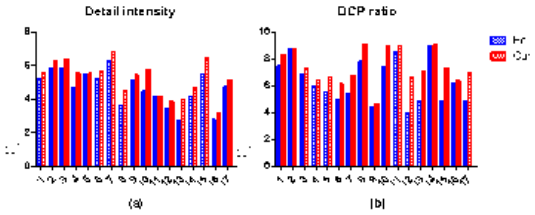

FIGURE 15. Image intrinsic property analysis.

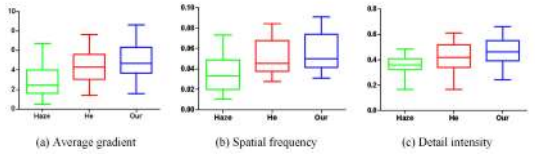

FIGURE 16. Comparison between our simplified algorithm and He's method.

values and used the ratio as a measure of haze residual. As shown in Fig.15, our results get more pixels with low DCP value which means our algorithm achieves better haze-free images. Also in Fig.15, the detail intensity [31] is used to measure how much information is retained in the image. It can be seen that our algorithm achieves better results, because our algorithm effectively avoids the halo effect, the final processing results restore more details.

In some cases, the images are not affected by noise. These images can be processed directly by RTV, and the template extracted in the main structure is calculated under a fixed α. Such a method will affect the anti-noise ability of the algorithm to a certain extent, but it simplifies the processing steps of the algorithm and reduces the parameters, and still maintains a good performance in halo effect and haze residual. We also took the images used in Fig.15 and used our simplified dehazing method to obtain the clear images. We then counted the average gradient, spatial frequency and detail intensity of the results and showed the Box-plot in Fig.16. It's clear that our simplified algorithm can still achieve better results than DCP.

VI. CONCLUSION

In this paper, we focus on the halo effect and the inaccurate transmission estimation in DCP and propose a Local Adaptive Template. The template is then used to improve the Dark Channel Prior algorithm and the Guided Filter algorithm respectively. It can effectively solve the block effect in DCP and the blur at the boundary in GF. After experiments on haze images, it is proved that the proposed algorithm can estimate the image transmission more accurately and avoid the halo effect effectively. Results of the proposed method are clearer and the haze removal is more thorough. Compared with the algorithms based on deep learning, our algorithm can get better clearing effect even in the case of heavy haze, and the color distribution of resulting clear image is closer to that of the original image. The indicators such as average gradient, spatial frequency and detail intensity are evaluated and prove that the our algorithm can achieve clearer and more realistic results containing more information.

REFERENCES

[1] N. S. Kopeika, "General wavelength dependence of imaging through the atmosphere," *Appl. Opt.*, vol. 20, no. 9, pp. 1532–1536, 1981.
[2] L. R. Bissonnette, "Imaging through fog and rain," *Proc. SPIE*, vol. 31, no. 5, pp. 1045–1053, 1992.
[3] Y. Yitzhaky, I. Dror, and N. S. KoPeika, "Restoration of atmospherically blurred images according to weather-predicted atmospheric modulation transfer function," *Opt. Eng.*, vol. 36, no. 11, pp. 3064–3072, 1997.
[4] Y. Xu, J. Wen, L. Fei, and Z. Zhang, "Review of video and image defogging algorithms and related studies on image restoration and enhancement," *IEEE Access*, vol. 4, pp. 165–188, 2015.
[5] M. Han, Z. Lyu, T. Qiu, and M. Xu, "A review on intelligence dehazing and color restoration for underwater images," *IEEE Trans. Syst., Man, Cybern., Syst.*, to be published.
[6] Z. Xu, X. Liu, and X. Chen, "Fog removal from video sequences using contrast limited adaptive histogram equalization," in *Proc. Int. Conf. Comput. Intell. Softw. Eng.*, Dec. 2009, pp. 1–4.
[7] D. D.-Y. Po and M. N. Do, "Directional multiscale modeling of images using the contourlet transform," *IEEE Trans. Image Process.*, vol. 15, no. 6, pp. 1610–1620, Jun. 2006.
[8] J. Wang, Q. Li, Z. Jia, N. Kasabov, and J. Yang, "A novel multi-focus image fusion method using PCNN in nonsubsampled contourlet transform domain," *Optik*, vol. 126, no. 20, pp. 2508–2511, 2015.
[9] Y. Li, J. Hu, and Y. Jia, "Automatic SAR image enhancement based on nonsubsampled contourlet transform and memetic algorithm," *Neurocomputing*, vol. 134, pp. 70–78, Jun. 2014.
[10] L. Tao and V. Asari, "Modified luminance based MSR for fast and efficient image enhancement," in *Proc. IEEE Appl. Imag. Pattern Recognit. Workshop*, Oct. 2003, vol. 4, no. 3, pp. 174–179.
[11] R. T. Tan, "Visibility in bad weather from a single image," in *Proc. IEEE Comput. Soc. Conf. Comput. Vis. Pattern Recognit.*, Jun. 2008, pp. 1–8.
[12] R. Fattal, "Single image dehazing," *ACM Trans. Graph.*, vol. 27, no. 3, 2008, Art. no. 72.
[13] K. He, J. Sun, and X. Tang, "Single image haze removal using dark channel prior," in *Proc. IEEE Comput. Soc. Conf. Comput. Vis. Pattern Recognit.*, Jun. 2009, pp. 1956–1963.
[14] K. He, J. Sun, and X. Tang, "Guided image filtering," *IEEE Trans. Pattern Anal. Mach. Intell.*, vol. 35, no. 6, pp. 1397–1409, Jun. 2013.
[15] S.-C. Pei and T.-Y. Lee, "Effective image haze removal using dark channel prior and post-processing," in *Proc. IEEE Int. Symp. Circuits Syst.*, May 2012, vol. 57, no. 1, pp. 2777–2780.
[16] J.-H. Kim, W.-D. Jang, J.-Y. Sim, and C.-S. Kim, "Optimized contrast enhancement for real-time image and video dehazing," *J. Vis. Commun. Image Represent.*, vol. 24, no. 3, pp. 410–425, 2013.
[17] Q. Yang, P. Ji, D. Li, S. Yao, and M. Zhang, "Fast stereo matching using adaptive guided filtering," *Image Vis. Comput.*, vol. 32, no. 3, pp. 202–211, 2014.

[18] L. Quan, Y. Hu, and M. Yan, "Cross-based adaptive guided filtering in image denoising," *J. Comput. Appl.*, vol. 35, no. 10, pp. 2959–2962, 2015.
[19] S. G. Narasimhan and S. K. Nayar, "Removing weather effects from monochrome images," in *Proc. IEEE Comput. Soc. Conf. Comput. Vis. Pattern Recognit.*, vol. 2, Dec. 2001, p. 2.
[20] J. E. Bresenham, "Algorithm for computer control of a digital plotter," *IBM Syst. J.*, vol. 4, no. 1, pp. 25–30, 1965.
[21] K. Zhang, J. Lu, and G. Lafruit, "Cross-based local stereo matching using orthogonal integral images," *IEEE Trans. Circuits Syst. Video Technol.*, vol. 19, no. 7, pp. 1073–1079, Jul. 2009.
[22] L. Xu, Q. Yan, Y. Xia, and J. Jia, "Structure extraction from texture via relative total variation," *ACM Trans. Graph.*, vol. 31, no. 6, 2012, Art. no. 139.
[23] R. Kimmel, M. Elad, D. Shaked, R. Keshet, and I. Sobel, "A variational framework for retinex," *Int. J. Comput. Vis.*, vol. 52, no. 1, pp. 7–23, 2003.
[24] J.-P. Tarel and N. Hautière, "Fast visibility restoration from a single color or gray level image," in *Proc. IEEE Int. Conf. Comput. Vis.*, Sep./Oct. 2009, pp. 2201–2208.
[25] B. Cai, X. Xu, K. Jia, C. Qing, and D. Tao, "DehazeNet: An end-to-end system for single image haze removal," *IEEE Trans. Image Process.*, vol. 25, no. 11, pp. 5187–5198, Nov. 2016.
[26] W. Ren, S. Liu, H. Zhang, J. Pan, X. Cao, and M.-H. Yang, "Single image dehazing via multi-scale convolutional neural networks," in *Proc. Eur. Conf. Comput. Vis.* Cham, Switzerland: Springer, 2016, pp. 154–169.
[27] C. O. Ancuti and C. Ancuti, "Single image dehazing by multi-scale fusion," *IEEE Trans. Image Process.*, vol. 22, no. 8, pp. 3271–3282, Aug. 2013.
[28] D. Berman, T. Treibitz, and S. Avidan, "Non-local image dehazing," in *Proc. IEEE Conf. Comput. Vis. Pattern Recognit. (CVPR)*, Jun. 2016, pp. 1674–1682.
[29] L. Shen, Y. Zhao, Q. Peng, J. C.-W. Chan, and S. G. Kong, "An iterative image dehazing method with polarization," *IEEE Trans. Multimedia*, vol. 21, no. 5, pp. 1093–1107, May 2019.
[30] N. Silberman, D. Hoiem, P. Kohli, and R. Fergus, "Indoor segmentation and support inference from RGBD images," in *Proc. Eur. Conf. Comput. Vis.* Berlin, Germany: Springer, 2012.
[31] D.-P. Li, J. Yu, and C. B. Xiao, "No-reference quality assessment method for defogged images," *J. Image Graph.*, vol. 16, no. 9, pp. 1753–1757, 2011.

LU XU received the B.S. degree in digital media technology from Northeastern University, China, in 2016, where he is currently pursuing the Ph.D. degree in pattern recognition and intelligent system. His research interests include image processing and image dehazing.

YING WEI received the B.S. degree from the Harbin Institute of Technology (HIT), China, in 1990, and the M.Sc. and Ph.D. degrees from Northeastern University, China, in 1997 and 2001, respectively, where she is currently a full-time Professor. Her research interests include image processing, pattern recognition, medical image computation and analysis, computer-aided diagnosis/detection (CAD), and computer vision. She has more than 50 journal articles and holds two granted patents in her research fields.

BIN HONG received the B.S. degree in automation from Northeastern University, China, in 2017, where he is currently pursuing the M.S. degree in pattern recognition and intelligent system. His research interests include image processing and image dehazing.

WEI YIN received the master's degree in pattern recognition and intelligent system from Northeastern University, China, in 2018. Her research interests include image processing and image dehazing.